Mass and Heat Transfer from or to a Single Sphere in Simple Extensional Creeping Flow

Jingsheng Zhang, Chao Yang, and Zai-Sha Mao
Key Laboratory of Green Process and Engineering, Institute of Process Engineering, Chinese Academy of Sciences, Beijing 100190, China

National Engineering Laboratory for Hydrometallurgical Cleaner Production Technology, Institute of Process Engineering, Chinese Academy of Sciences, Beijing 100190, China

DOI 10.1002/aic.12811
Published online November 21, 2011 in Wiley Online Library (wileyonlinelibrary.com).

The first detailed numerical investigation on the mass and heat transfer both outside and inside a solid or liquid sphere immersed in a simple extensional flow for a larger range of Peclet numbers (1–100,000) is presented. By making use of the known Stokes velocity field at small Reynolds numbers, a finite difference method with the control volume formulation is adopted to solve the convection-diffusion transport equation. Simulation results show that the transport rate, which is represented by Sherwood number, is significantly affected by Peclet number and viscosity ratio. The flow direction, no matter a uniaxial extensional flow or a biaxial extensional flow, has no effect on the total transport rate but affects the concentration distribution a lot. Some comparisons between present simulations and previous studies are made to validate each other and confirm the reliability and applicable scopes of reported correlations. A few new correlations are put forward to predict the transfer rate at finite Peclet numbers for various values of viscosity ratios. *AIChE J,* 58: 3214–3223, 2012
Keywords: mass and heat transfer, sphere, extensional flow, creeping flow, numerical simulation

Introduction

The problem of mass and heat transfer between a single sphere and an ambient fluid is of great importance in chemical and processing industry: here, the sphere can be a bubble, a liquid drop, or a solid particle. The knowledge of the relevant fluid dynamics and of the transport process from or to a single sphere is the basis for quantifying the transport behavior in a system with many spheres, and hence, is crucial for designing process equipments. Because of its significance, extensive experimental investigations,[1–3] theoretical studies,[4–14] and numerical simulations[15–19] have been carried out to solve this problem in the past.

As well-known, high-viscosity liquids, such as fibrous polymer solution, foods, and biological materials, are usually processed in rotary machines, under conditions in which extensional flows exist. For example, if we form a fiber dosed with nanoparticles by electrospinning or fiber drawing, the flow in the fiber is of the nature of a uniaxial extensional flow, whereas in the compression molding to form composite polymer sheets, one usually has approximately a biaxial extensional flow. On the other hand, in some polymer blend systems, due to the concentration or temperature difference between the dispersed particles and the continuous liquid, the mass or heat transport occurs, which will eventually affect the structural properties of polymer blends. Therefore, the investigation on the mass and heat transfer between a small particle and the surrounding fluid which is subject to extensional flows has both scientific and industrial significances.

To our knowledge, the relevant investigation on the transport problem in an extensional flow was initially carried out by Gupalo and Riazantsev,[20] who treated the steady mass transfer from a sphere in the creeping fluid flow at high Peclet numbers ($Pe = |E|a^2/D$, here E is the strength of the extension rate, a is the radius of the sphere, and D is the diffusivity). They solved the problem in the approximation of diffusion boundary layer and their solution shows that the Sherwood number ($Sh = ka/D$, here k is the mass-transfer coefficient) was proportional to $Pe^{1/3}$ for a solid sphere but to $Pe^{1/2}$ for a liquid drop. After that, Bachelor[21] studied the mass transfer from a solid sphere suspended in a steady linear flow fluid and derived the analytical expressions for Sh at both small and high Pe. Morrison[22] solved the transient transport problem in the extensional creeping flow regime by considering a more general case that the transport resistances both inside and outside the drop were important, and found Sh was related to $Pe^{1/2}$ as well as the diffusivity/conductivity ratio. Considering the deformation of a bubble in an extensional creeping flow, Favelukis et al.[23–25] solved the mass transfer from a slender bubble and got an analytical solution.

The aforementioned results,[20–25] however, are all analytical solutions and hence restricted to the situation that Pe is

Correspondence concerning this article should be addressed to C. Yang at chaoyang@home.ipe.ac.cn.

far larger or far smaller than unity. To examine the transport behavior at intermediate *Pe*, Kurdyumov and Polyanin[26] calculated the steady mass transfer from a sphere in an extensional creeping flow numerically for a wide range of *Pe*. They proposed some approximate correlations of *Sh*, which represented very well their calculations. However, the maximum *Pe* shown in their study is 2000 and only a few numerical results were given in their paper to validate their approximate correlations, perhaps not enough to derive a reliable correlation. Thus, to make sure these correlations can be applied reliably, it is necessary to check them with more numerical results. On the other hand, Kurdyumov and Polyanin[26] only considered the transport processes outside a sphere, in which the internal transport resistance was negligible. However, there are still many industrial processes such as liquid–liquid extraction and droplets experiencing condensation at the interface, where the transport process in the continuous phase can be considered quasi-steady, whereas the one inside the drop must always be treated as a transient process because of the limited inventory of solute in a liquid sphere. In these cases, the transport resistance is reasonably considered to exist mainly inside the liquid sphere and hence the characteristics of the entire conjugate transport rest on the disperse phase, particularly in the latter period of the transport process. In this sense, the relevant investigation on the transport behavior inside a liquid sphere, which is the so-called internal problem, is also practically significant.

In this study, we use a finite difference method to examine the mass and heat transfer from or to a single sphere immersed in a simple extensional creeping flow at Peclet numbers between 1 and 100,000, which are in a sufficiently wide range for industrial applications. Here, the single sphere refers to a solid particle and a liquid drop, and both the uniaxial and biaxial extensional flows are considered. Two goals are pursued in this study: first, to check the reliability of approximate correlations derived by Kurdyumov and Polyanin[26] by calculating the mass and heat transfer outside a sphere; second, to examine the transport behavior inside a liquid drop at finite *Pe* because no numerical simulation is to date available in the literature. In this article, some comparisons between present simulations and previous analytical solutions are made to validate each other. Besides the transport rates, the concentration fields are also examined, from which the transport behavior can be understood more clearly.

Flow Field of Simple Extensional Creeping Flow

For the case of a spherical drop fixed in a planar creeping flow of large extent, the velocity field has been well-documented[27] and given by

$$\mathbf{u}_1 = \Gamma\cdot\mathbf{r} - \frac{\lambda}{(\lambda+1)r^5}\mathbf{E}\cdot\mathbf{r} - \left[\frac{(5\lambda+2)}{2(\lambda+1)}\frac{1}{r^5} - \frac{5\lambda}{2(\lambda+1)}\frac{1}{r^7}\right]\times(\mathbf{r}\cdot\mathbf{E}\cdot\mathbf{r})\mathbf{r} \quad (1)$$

$$\mathbf{u}_2 = \Omega\cdot\mathbf{r} + \left[-\frac{3}{2(\lambda+1)} + \frac{5r^2}{2(\lambda+1)}\right]\mathbf{E}\cdot\mathbf{r} - \frac{1}{(\lambda+1)}(\mathbf{r}\cdot\mathbf{E}\cdot\mathbf{r})\mathbf{r} \quad (2)$$

where subscript 1 refers to the continuous phase and 2 the drop phase, $\mathbf{r}$ is the position vector, λ is the viscosity ratio of the drop to the continuous fluid, Γ is the transpose of the velocity gradient tensor, and $\mathbf{E}$ and Ω are the rate of strain tensor and the transpose of the vorticity tensor of the ambient linear flow, respectively. Note that $\lambda\to\infty$ corresponds to the case of solid sphere. For the particular geometry that a single sphere of radius a immersed in a simple extensional creeping flow, $\Omega = \mathbf{0}$ and

$$\Gamma = \mathbf{E} = \begin{pmatrix} -\frac{1}{2} & 0 & 0 \\ 0 & -\frac{1}{2} & 0 \\ 0 & 0 & 1 \end{pmatrix} E \quad (3)$$

where E characterizes the extension strength, which is positive for the uniaxial case and negative for the biaxial case. Scaling Eqs. 1 and 2 by $|E|a$, the flow velocity in dimensionless form in a spherical coordinate system (r, θ, φ), with the sphere center at the origin, the azimuthal angle θ measured relative to the z axis, and ϕ measured between the projection of the position vector into the x-y plane and the x axis, is

$$\begin{aligned} u_{1r} &= \pm\left(1-\frac{3}{2}\sin^2\theta\right)\left(r - \frac{5\lambda+2}{2(\lambda+1)r^2} + \frac{3\lambda}{2(\lambda+1)r^4}\right) \\ u_{1\theta} &= \mp\frac{3}{2}\sin\theta\cos\theta\left(r - \frac{\lambda}{(\lambda+1)r^4}\right) \\ u_{1\varphi} &= 0 \end{aligned} \quad (4)$$

$$\begin{aligned} u_{2r} &= \pm(1-\frac{3}{2}\sin^2\theta)\left(-\frac{3r}{2(\lambda+1)} + \frac{3r^3}{2(\lambda+1)}\right) \\ u_{2\theta} &= \mp\frac{3}{2}\sin\theta\cos\theta\left(-\frac{3r}{2(\lambda+1)} + \frac{5r^3}{2(\lambda+1)}\right) \\ u_{2\varphi} &= 0 \end{aligned} \quad (5)$$

where the upper and lower signs correspond to the uniaxial extensional flow and the biaxial one, respectively. The simple extensional flow is axisymmetric, with no dependence on φ.

Figure 1 depicts the streamlines both outside and inside a sphere in the uniaxial extensional flow. It can be seen from Figure 1a that there are two sets of streamlines along the drop surface, both of which emanate from the equator ($\theta = \pi/2$) and flow toward one of the poles ($\theta = 0$ and $\theta = \pi$). This just shows the characteristics of a uniaxial extension that the fluid stretches along the z axis and contracts on the x-y plane. Subject to such a strain stress on the surface, as shown in Figure 1b, the axisymmetric circulation is formed inside the drop. For the biaxial extension case, streamline patterns are the same as those shown in Figure 1 but with an opposite flow direction, i.e., the fluid at the surface becomes flowing from the poles to the equator.

Governing Equations of Mass and Heat Transfer and Scheme of Numerical Simulation

The mass-transfer processes both inside and outside the sphere are governed by the general convection-diffusion equation:

$$\frac{\partial c_i}{\partial t} + \mathbf{u}_i\cdot\nabla c_i = D_i\nabla^2 c_i \quad (6)$$

where c is the solute concentration, D is the mass diffusivity, and the subscript refers to the continuous phase ($i = 1$) and the drop phase ($i = 2$). The concentration fields are axisymmetric (irrelevant of φ) because the flow and the outer boundary conditions are axisymmetric. An energy equation describing temperature distributions would obey an equation of the same nature, so there is no need to address heat transfer separately.

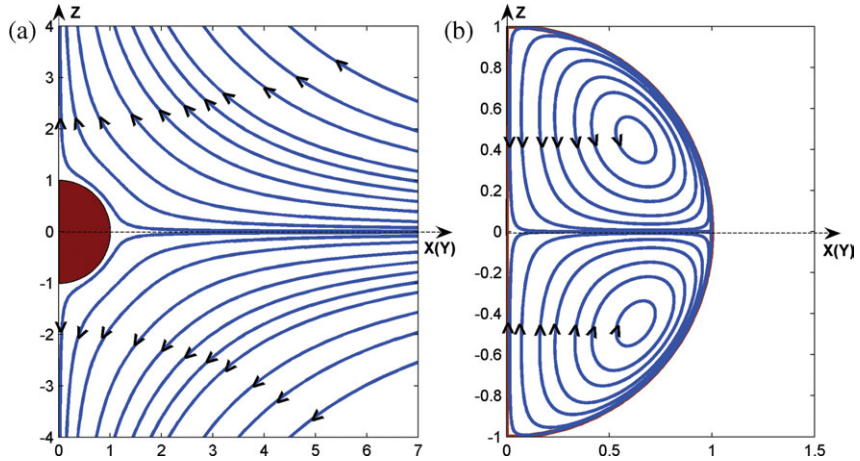

Figure 1. Flow field for a sphere immersed in a uniaxial extensional flow ($\lambda = 1$).

(a) Streamlines outside a sphere and (b) streamlines inside a sphere. [Color figure can be viewed in the online issue, which is available at wileyonlinelibrary.com.]

In this study, some simple assumptions are considered valid:

1. Both the dispersed (liquid drop) and continuous phases are Newtonian;
2. The shape of the particle remains spherical;
3. The physical properties including mass diffusivity, fluid viscosity, and density are constant and mass transfer does not affect flow structure.

Under these assumptions, Eq. 6 for an axisymmetric mass transfer problem can be expressed in a spherical coordinate system (r, θ) in the dimensionless form as

$$\frac{\partial C_i}{\partial \tau} + \frac{1}{r^2}\frac{\partial}{\partial r}(r^2 u_{ir} C) + \frac{1}{r\sin\theta}\frac{\partial}{\partial \theta}(u_{i\theta}\sin\theta C_i) = \frac{1}{Pe_i}\left[\frac{1}{r^2}\frac{\partial}{\partial r}\left(r^2\frac{\partial C_i}{\partial r}\right) + \frac{1}{r\sin\theta}\frac{\partial}{\partial\theta}\left(\frac{1}{r}\sin\theta\frac{\partial C_i}{\partial\theta}\right)\right] \tag{7}$$

where C_i is the dimensionless concentration, $\tau = |E|t$ is the dimensionless time, and $Pe_i = |E|a^2/D_i$ is the Peclet number that indicates the relative strength of convective transport to diffusive transport.

In general, both the dissolution equilibrium of solute and the continuity of mass flux should be satisfied on the sphere surface during the whole transport process, i.e.,

$$D_1\left.\frac{\partial c_1}{\partial r}\right|_{r=1} = D_2\left.\frac{\partial c_2}{\partial r}\right|_{r=1}; \qquad c_2^s = mc_1^s \tag{8}$$

where m is the distribution coefficient of the solute in two liquids and superscript s refers to the sphere surface. As only the mass transfer outside or inside a sphere is considered, Eq. 8 reduces to simpler forms.

For the steady mass transfer outside a sphere, which corresponds to the case that the Biot number ($Bi = ka/mD_2$) is small enough to neglect the internal transport resistance, the concentration of the drop can be taken as uniform and constant approximately and hence c_1^s is also uniform and constant. On the other hand, the concentration field far from the sphere, c_∞, is undisturbed and always maintains a constant. Assuming $c_\infty < c_1^s$, the solute will be transported from the sphere to the ambient fluid. In this case, in terms of the dimensionless concentration defined by $C_1 = (c_1 - c_\infty)/(c_1^s - c_\infty)$, Eq. 8 is simplified to

$$r = 1, \quad C_1 = C_1^s = 1 \tag{9}$$

and the boundary condition far from the sphere is given by

$$r \to \infty, \quad C_1 = C_\infty = 0 \tag{10}$$

For the transient transport inside a drop which is suitable for the case that Bi is sufficiently large to neglect the external transport resistance. On the contrary, the concentration in the whole ambient fluid is roughly uniform and constant, and thus c_2^s can be regarded as uniform and constant at any time. Assume that the initial concentration inside the drop, c_0, is uniform but lower than c_2^s, the solute will be transported from the drop surface to the intra of the drop. In terms of $C_2 = (c_2 - c_0)/(c_2^s - c_0)$, Eq. 8 is simplified as

$$\tau \geq 0 \quad \text{and} \quad r = 1\,, \quad C_2 = C_2^s = 1 \tag{11}$$

and other initial and boundary conditions can be expressed by

$$\tau = 0 \ \text{ and } \ r<1, \qquad C_2 = 0 \tag{12}$$

$$\tau \geq 0 \ \text{ and } \ r = 0, \quad \frac{\partial C_2}{\partial r} = 0 \tag{13}$$

For both the external and internal transport processes, the symmetry condition $\partial C_i/\partial\theta = 0$ is applied at the z axis ($\theta = 0$ and $\theta = \pi$).

In this study, making use of the known velocity filed in Eqs. 4 and 5, a finite difference method is used to solve the convection-diffusion equation. The computational domain is $0 \leq r \leq R$ and $0 \leq \theta \leq \pi$, where R is the size of the outer boundary in the radial direction. Equation 7 is discretized on a grid, which is uniform in the polar (θ) direction, but nonuniform in the radial (r) direction. For the external grid, 10–20 nodes in r direction are allocated densely and uniformly near the sphere since the concentration varies rapidly in this region, but after that an exponential relation, $r(n) = r(n-1)e^{\alpha}$, is applied to determine the nth node away from the sphere, where α is a small constant used to adjust the grid spacing. For the internal grid, there are similarly 10–20 dense and uniform nodes in the r direction near the sphere surface, whereas the nodes away from the surface are also uniform but with a larger grid spacing. A fifth-order WENO (weighted essentially

nonoscillatory) scheme in spatial discretization and a third-order TVD (total variation diminishing) Runge–Kutta scheme in time are adopted for solving Eq. 7 with sufficient accuracy.[28] The transient calculation of mass transfer can be taken as reaching the steady state if the change in Sherwood number during the latest 1/5 of the computational time is less than 1%.

At high Pe, a concentration boundary layer is formed near the sphere surface and it becomes thinner with increasing Pe. Thus, the grid near the sphere surface should be much finer at high Pe. The grid sensitivity analysis in this work reveals that a grid of $135(r) \times 40(\theta)$ ($\Delta r = 0.00125$ and $R = 40$) for the solid sphere case and a grid of $200(r) \times 40(\theta)$ ($\Delta r = 0.0005$ and $R = 40$) for the liquid drop case, respectively, suffice for computing the steady external mass transfer at Pe_1 up to 100,000, where Δr is the smallest grid size in the radial direction near the sphere surface. For the mass transfer inside a liquid drop, a grid of $60(r) \times 60(\theta)$ ($\Delta r = 0.0005$) is sufficient for getting accurate results at Pe_2 up to 100,000. A constant time step is employed for each run with the time step ranging between $\Delta\tau = 2.5 \times 10^{-7}$ at $Pe_i = 1$ to $\Delta\tau = 5 \times 10^{-3}$ at $Pe_i = 100{,}000$.

Mass Transfer Outside a Solid Sphere

Comparison between present simulations and previous studies

For the steady mass transfer from a solid sphere, the analytical correlation applicable to high Pe_1 was given by Bachelor[21] and Gupalo and Riazantsev[20] as follows:

$$Sh = 0.968\, Pe_1^{1/3} \tag{14}$$

The Sherwood number Sh is calculated by

$$Sh = \frac{1}{2\Delta C_1} \int_{\theta=0}^{\theta=\pi} \left(-\frac{\partial C_1}{\partial r}\bigg|_{r=1} \right) \sin\theta \, d\theta \tag{15}$$

where $\Delta C_1 = C_1^s - C_\infty = 1$ characterizes the driving force of mass transfer. As well-known, $Sh = 1$ for the purely conductive mass transfer from a sphere at $Pe_1 = 0$.[21]

As it is difficult to obtain an analytical prediction for the transfer rate at finite Pe_1, Kurdyumov and Polyanin[26] simulated numerically this problem and proposed a correlation applied to the entire range of Pe_1 as follows:

$$Sh = 0.5 + (0.125 + 0.745 Pe_1)^{1/3} \tag{16}$$

The simulated Sh for a solid sphere in a uniaxial extensional flow as well as the results calculated by Eqs. 14 and 16 are given in Figure 2. It shows that present simulations agree with Eq. 16 well with a maximum deviation of 3.5% for $Pe_1 \leq 30{,}000$, but the deviation becomes large when Pe_1 surpasses 30,000 and increases with the increase of Pe_1. The present simulations, however, are quite close to Eq. 14 with a relative deviation less than 2.5% for $Pe_1 > 30{,}000$. On the other hand, as shown in Figure 2b, Eq. 14 departs from our simulations a lot at low Pe_1. In this sense, we recommend using Eq. 16 for $Pe_1 < 30{,}000$ and adopting Eq. 14 for $Pe_1 > 30{,}000$ to ensure a more accurate prediction.

Further analysis on transport phenomena

The dimensionless concentration contours around a solid sphere immersed in a uniaxial extension flow are given in Figure 3. Two general observations can be made by examining this figure. First, as the solute is transported by both convection and diffusion in the flow direction, it can be distributed to a large extent along the z axis. However, due to the surrounding fluid flowing toward the sphere near the x-y plane, the solute is mainly carried away from the sphere by diffusion and hence it is only distributed to a limited extent at this region. In other words, the thickness of the concentration boundary layer surrounding the sphere is the thinnest on the x-y plane and keeps growing from the x-y plane to the two poles. In the small neighborhoods of the two poles, as presented in the theoretical study,[20] the thickness of the concentration boundary layer is large and approaches an infinite value when $\theta \to 0$ and $\theta \to \pi$. A thick concentration boundary layer indicates a small concentration gradient, so the local mass flux from the sphere should increase from the two poles to the x-y plane. Second, the concentration boundary layer not very close to the two poles becomes thinner with increasing Pe_1, which will lead to a higher total mass flux on the sphere surface.

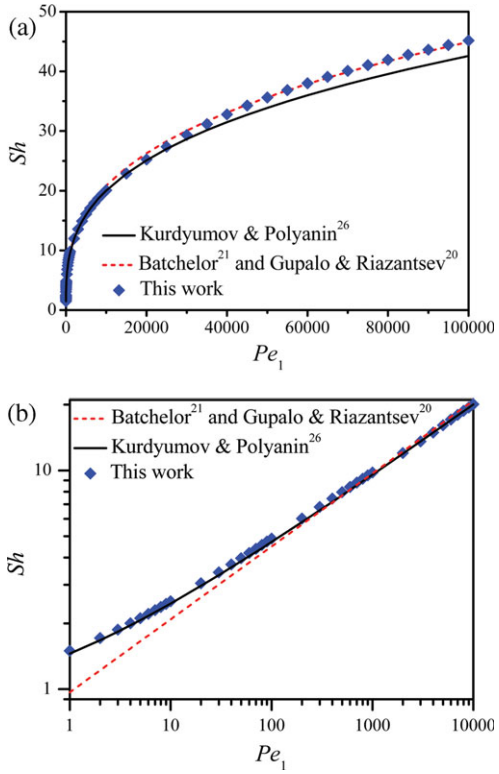

Figure 2. Variation of *Sh* with Pe_1 for mass transfer from a solid sphere in a uniaxial extensional flow.

(a) A plot on a linear–linear scale and (b) a plot on a logarithm–logarithm scale. [Color figure can be viewed in the online issue, which is available at wileyonlinelibrary.com.]

The local $\partial C_1/\partial r$ on the sphere surface derived from the boundary layer theory[20,21] at high Pe_1 is given by

$$-\partial C_1/\partial r = \frac{(5/6)^{1/3}}{\Gamma(4/3)} \sin\theta |\cos\theta|^{1/2} A^{-1/3}(\theta) Pe_1^{1/3} \tag{17}$$

where Γ is the gamma function and $A(\theta)$ can be expressed as follows:

$$A(\theta) = \begin{cases} H(\theta), & 0 \leq \theta \leq \pi/2 \\ H(\pi - \theta), & \pi/2 \leq \theta \leq \pi \end{cases} \tag{18}$$

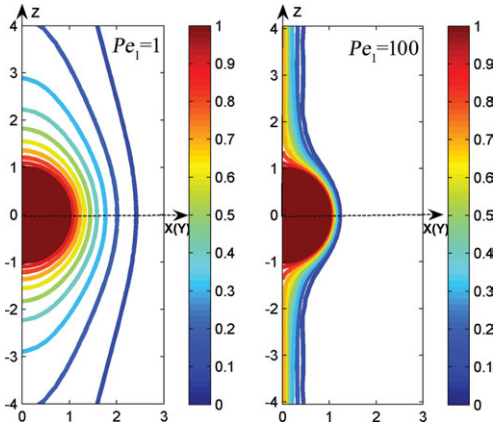

Figure 3. Concentration contours around a solid sphere in a uniaxial extensional flow (the difference of dimensionless concentration between two adjacent lines is 0.1).

[Color figure can be viewed in the online issue, which is available at wileyonlinelibrary.com.]

For the uniaxial extension, we have

$$H(\theta) = \frac{1}{5}\frac{1}{(2\pi)^{3/2}}\frac{1}{\Gamma^2(5/4)} + \frac{2}{5}\sin\theta\cos^{3/2}\theta - \frac{4}{5}E(\theta/2, \sqrt{2}) \tag{19}$$

in which $E(\theta/2, \sqrt{2})$ is the elliptic integral of the second kind. Equation 17 reveals that the term of $(-\partial C_1/\partial r)/Pe_1^{1/3}$ has the same dependence on θ at different Pe_1. This conclusion is validated by the present simulations. As shown in Figure 4, the simulated $(-\partial C_1/\partial r)/Pe_1^{1/3}$ approaches gradually the theory with increasing Pe_1, and the results at different Pe_1 coincide with each other well when Pe_1 surpasses ~1000. Moreover, in accordance with the trend revealed in Figure 3, Figure 4 shows that the local $\partial C_1/\partial r$ increases with θ rising from 0 to $\pi/2$ at a given Pe_1.

For the mass transfer from a sphere immersed in a simple extensional flow, the reported theoretical analysis[20,21] concluded that the flow field, no matter a uniaxial extension or a biaxial one, had no effect on the total transfer rate due to the linearity of the governing equations. The simulated *Sh* representing the total mass-transfer rate are shown in Figure 5, which clearly confirms this conclusion if the slight numerical errors are ignored.

Although the flow direction has been proved having no effect on the total mass flux, it should affect the concentration distribution a lot because the convective transport is dominated by the fluid flow. Figures 6 and 7 show the concentration field and the variation of local $\partial C_1/\partial r$ for the biaxial extension case. As depicted in Figure 6, the concentration field in the biaxial extension is in a contrary manner compared with that in the uniaxial extension, i.e., the maximum thickness of concentration boundary layer appears at $\theta = \pi/2$ and it becomes decreasing from the *x*-*y* plane to the two poles. Such a concentration field, as shown in Figure 7, makes $\partial C_1/\partial r$ increasing from the *x*-*y* plane to the two poles. This difference in the concentration or temperature distributions is important in industrial processes because it may greatly affect the components and structural properties of a polymer blend. Except the above difference, similar to the uniaxial extension, the thickness of concentration boundary layer not close to the limit value of $\theta = \pi/2$ also keeps reducing with increasing Pe_1. In addition, the local concentration gradient derived from the boundary layer

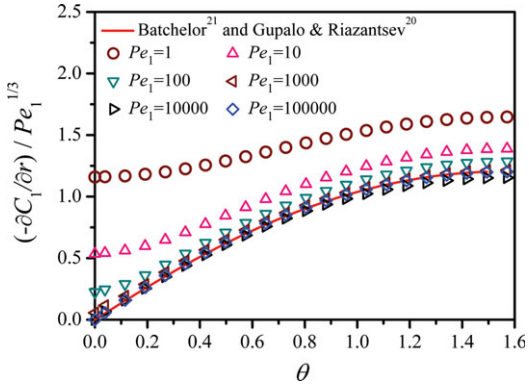

Figure 4. Local concentration gradient $(-\partial C_1/\partial r)/Pe_1^{1/3}$ on solid sphere surface as a function of θ in a uniaxial extensional flow.

[Color figure can be viewed in the online issue, which is available at wileyonlinelibrary.com.]

theory[20,21] for the biaxial extension case is similarly determined by Eq. 17 except for some changes in the expression of $H(\theta)$:

$$H(\theta) = \frac{2}{5}\sin\theta\cos^{3/2}\theta - \frac{4}{5}E(\theta/2, \sqrt{2}) \tag{20}$$

As one expects, Figure 7 shows that the simulations become more and more close to the reported theory as Pe_1 increases gradually.

Mass Transfer Outside a Liquid Sphere

Comparison between present simulations and previous studies

For the mass transfer from a spherical drop immersed in a simple extensional flow, the analytical solution applicable to high Pe_1 derived by Gupalo and Riazantsev[20] is

$$Sh = \sqrt{\frac{3}{2\pi(\lambda+1)}}Pe_1^{1/2} \tag{21}$$

Equation 21 indicates that *Sh* is related to the viscosity ratio λ and proportional to $Pe_1^{1/2}$ for the liquid-drop case instead of $Pe_1^{1/3}$ for the solid-sphere case due to the

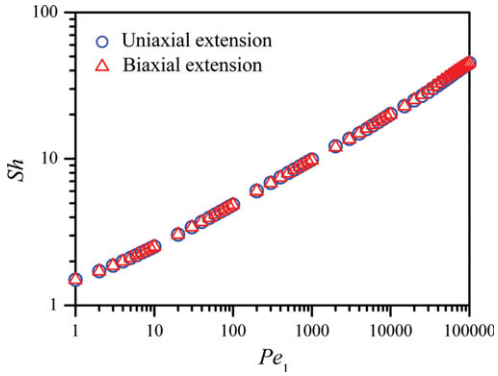

Figure 5. Variation of *Sh* with Pe_1 for mass transfer from a solid sphere in a simple extensional flow.

[Color figure can be viewed in the online issue, which is available at wileyonlinelibrary.com.]

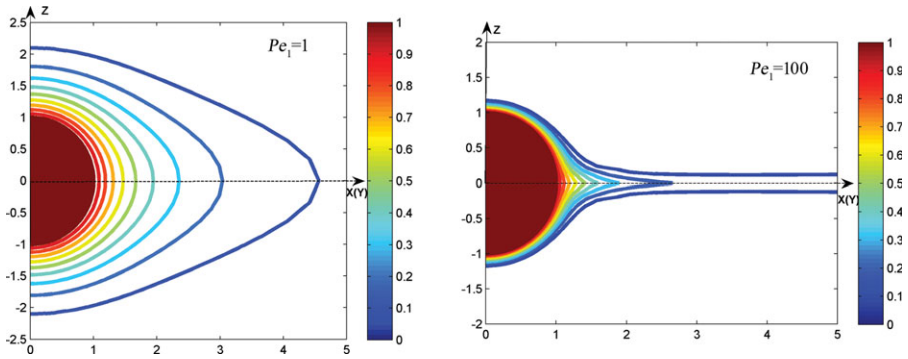

Figure 6. Concentration contours around a solid sphere in a biaxial extensional flow at different Pe_1.

[Color figure can be viewed in the online issue, which is available at wileyonlinelibrary.com.]

difference between the fluid motion near a solid particle and that near a liquid drop.

For the uniaxial extension case, we compare Sh between present simulations and Eq. 21 in the range of $50{,}000 \leq Pe_1 \leq 100{,}000$ in Figure 8. It shows that present simulations and theoretical predictions are in good agreement for the cases of $\lambda = 0.1$ and $\lambda = 1$. The slopes of Sh against $Pe_1^{1/2}$ obtained from our simulations are about 0.658 for $\lambda = 0.1$ and 0.493 for $\lambda = 1$, which are all very close to the theoretical values of 0.659 and 0.487, respectively. However, the simulated Sh is always larger than the theoretical prediction for the case of $\lambda = 20$, and the fitting slope of 0.184 deviates from the theoretical value of 0.151 a lot. We presume the large deviation at $\lambda = 20$ resulted from the fact that the value of Pe_1 used in Figure 8 is not high enough to apply the approximation of concentration boundary layer. This presumption is validated by our simulations at much high Pe_1. As can be seen in Table 1, our simulations approach the theory gradually with increasing Pe_1, and the fitting slope of 0.157 obtained at $250{,}000 \leq Pe_1 \leq 300{,}000$ is already very close to the theoretical value of 0.151. Such results shown in Figure 8 and Table 1 reveal a fact that the lower limit of Pe_1 at which Eq. 21 works well should become higher gradually with the increase of λ.

Kurdyumov and Polyanin[26] proposed two approximate correlations to calculate Sh for the liquid drop case. The first one is applicable for $0 \leq Pe_1 \leq 200$ and given by

$$Sh = \frac{1}{\lambda+1}\left[0.6 + (0.16 + 0.48Pe_1)^{1/2}\right] + \frac{\lambda}{\lambda+1}\left[0.5 + (0.125 + 0.745Pe_1)^{1/3}\right] \quad (22)$$

The other is a cubic equation, of which the positive root is applied to predict Sh at higher Pe_1:

$$Sh^3 - \frac{3Pe_1}{2\pi(\lambda+1)}Sh - 0.745Pe_1 = 0 \quad (23)$$

Kurdyumov and Polyanin[26] suggested that Sh at any value of Pe_1 can be gotten by using Eqs. 22 and 23, but they used only a few computing data to validate their conclusion. Therefore, it is necessary to check the accuracy of these two equations.

By examining Eq. 1, it is easy to deduce that Sh decreases with increasing λ due to the small flow velocity at large λ. Considering Eq. 22, however, Sh does not decrease monotonically with λ. In terms of $\partial Sh/\partial\lambda = 0$, one can easily get the conclusion that Sh increases with λ when $Pe_1 < 2.316$, which obviously contradicts with the truth. The results of Sh

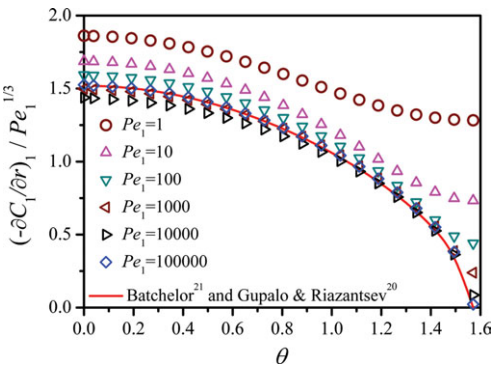

Figure 7. Local concentration gradient $(-\partial C_1/\partial r)/Pe_1^{1/3}$ on solid sphere surface as a function of θ in a biaxial extensional flow.

[Color figure can be viewed in the online issue, which is available at wileyonlinelibrary.com.]

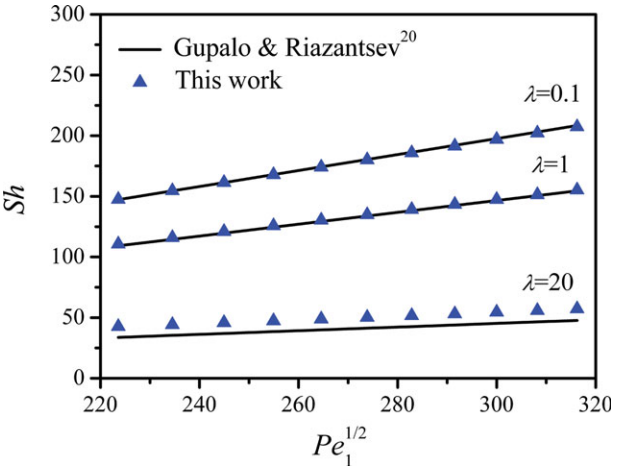

Figure 8. Variation of Sh with $Pe_1^{1/2}$ for mass transfer from a liquid drop in a uniaxial extensional flow in the range of $50{,}000 \leq Pe_1 \leq 100{,}000$.

[Color figure can be viewed in the online issue, which is available at wileyonlinelibrary.com.]

Table 1. Fitting Slope of Sh Against $Pe_1^{1/2}$ Obtained from Present Simulations for $\lambda = 20$

Range of Pe_1	Fitting Slope of Sh Against $Pe_1^{1/2}$
$10{,}000 \le Pe_1 \le 50{,}000$	0.201
$50{,}000 \le Pe_1 \le 100{,}000$	0.184
$100{,}000 \le Pe_1 \le 150{,}000$	0.167
$150{,}000 \le Pe_1 \le 200{,}000$	0.161
$200{,}000 \le Pe_1 \le 250{,}000$	0.158
$250{,}000 \le Pe_1 \le 300{,}000$	0.157

for $1 \le Pe_1 \le 10$ are given in Table 2, showing that Eq. 22 is indeed not accurate enough to predict Sh at small Pe_1, especially for small values of λ.

The comparison between present simulations and Kurdyumov and Polyanin's results[26] is show in Figure 9. It can be seen that Eq. 22 is in reasonable agreement with our simulations at lower Pe_1 and the deviation is roughly less than 5% when Pe_1 is larger than 10 but less than 1000 for all the values of $\lambda = 0.1$, 0.5, 1, 5, 10, 20, 50, and 100 computed in this work. Therefore, we think Eq. 22 can be used to predict Sh at $10 < Pe_1 \le 1000$ with acceptable errors, which is a larger range than that suggested by Kurdyumov and Polyanin,[26] namely, $Pe_1 \le 200$. Figure 9 also reveals that Eq. 23 departs from present simulations in a large extent at small Pe_1, but the deviation decreases with increasing Pe_1 and reduces to be within 5% when Pe_1 surpasses 1000 for all the eight values of λ. In this way, Eq. 23 is applicable for calculating Sh for $Pe_1 > 1000$.

As Eq. 22 is not accurate at small Pe_1, one correlation applicable for $1 \le Pe_1 \le 10$ with relative errors less than 1.5% is acquired according to present simulations:

$$Sh = \frac{1}{\lambda+1}\left(0.207Pe_1^{1/2} - 0.201\right) + 0.467Pe_1^{1/2} + 1.053 \tag{24}$$

Further, a new correlation is proposed to replace Eq. 23 by making some corrections to Eq. 22 because Eq. 23 is an implicit cubic equation and inconvenient to be used directly:

$$Sh = \frac{1}{\lambda+1}\left[0.6 + (0.16 + 0.48Pe_1)^{1/2}\right] + \frac{\lambda}{\lambda+1}\left[0.5 + (0.125 + 0.745Pe_1)^{1/3}\right] + f_1 + f_2\exp(-Pe_1^{1/6}/f_3) \tag{25}$$

The fitting parameters in Eq. 25 are related to the viscosity ratio and given by

$$f_1 = -19.844 + 17.846\frac{1}{\lambda+1} + 19.491\exp\left(\frac{-2.174}{\lambda+1}\right) \tag{26}$$

$$f_2 = -1.781 + 2.746\exp\left[-\left(\frac{1.336}{\lambda+1} - 0.664\right)^2\right] \tag{27}$$

$$f_3 = -1.478 - 0.371\exp(-0.274\lambda) - 0.251\exp(-0.072\lambda) \tag{28}$$

For $Pe_1 > 1000$, the relative error is approximately less than 3% between Eqs. 23 and 25 and less than 5% between Eq. 25 and present simulations.

Further analysis on transport phenomena

Because of the qualitative similarity of flow field, the concentration distribution around a liquid drop for any fixed λ resembles that around a solid sphere. The effect of λ on the concentration field that the concentration boundary layer surrounding the drop becomes thinner with decreasing λ is also comprehensible since the convection is strong at small λ. In addition, Gupalo and Riazantsev[20] showed that the analytical $\partial C_1/\partial r$ on the drop surface for the uniaxial extension was determined by

$$-\partial C_1/\partial r = \sqrt{\frac{6}{\pi(1+\lambda)(1-\sin^4\theta)}}\sin^2\theta|\cos\theta|Pe_1^{1/2} \tag{29}$$

The simulated $(-\partial C_1/\partial r)/Pe_1^{1/2}$ for $\lambda = 1$ is given in Figure 10. As one expects, the simulations become more and more consistent as well as close to the theory as Pe_1 increases gradually. In addition, similar to the solid sphere case, both the theoretical analysis[20] and present simulations validate that the total transport rate from a liquid drop in a biaxial extensional flow remains the same as that in a uniaxial extensional flow.

Mass Transfer Inside a Liquid Sphere

The transient mass-transfer rate inside a liquid sphere without resistance in the ambient fluid can be represented by the instantaneous Sherwood number:

$$Sh = \frac{1}{2\Delta C_2}\int_{\theta=0}^{\theta=\pi}\left(\left.\frac{\partial C_2}{\partial r}\right|_{r=1}\right)\sin\theta\, d\theta \tag{30}$$

where $\Delta C_2 = C_2^s - \overline{C}_d$ is the driving force and $\overline{C}_d$ is the average bulk concentration of the drop at any instant which can be obtained by

Table 2. Sh in the Range of $1 \le Pe_1 \le 10$ for Three Different Values of λ

	$\lambda = 0.1$			$\lambda = 1$			$\lambda = 10$		
Pe_1	This Work	Equation 22	Relative Deviation	This Work	Equation 22	Relative Deviation	This Work	Equation 22	Relative Deviation
1	1.534	1.405	−8.4%	1.517	1.427	−5.9%	1.500	1.450	−3.4%
2	1.797	1.660	−7.6%	1.757	1.666	−5.2%	1.719	1.672	−2.8%
3	2.004	1.862	−7.1%	1.941	1.848	−4.8%	1.883	1.834	−2.6%
4	2.180	2.035	−6.7%	2.096	2.001	−4.5%	2.017	1.966	−2.5%
5	2.336	2.188	−6.3%	2.231	2.134	−4.4%	2.132	2.079	−2.5%
6	2.477	2.327	−6.0%	2.351	2.253	−4.2%	2.234	2.179	−2.5%
7	2.607	2.455	−5.8%	2.463	2.362	−4.1%	2.326	2.269	−2.5%
8	2.728	2.575	−5.6%	2.565	2.463	−4.0%	2.410	2.351	−2.5%
9	2.842	2.688	−5.4%	2.661	2.557	−3.9%	2.488	2.426	−2.5%
10	2.949	2.794	−5.3%	2.751	2.646	−3.8%	2.561	2.497	−2.5%

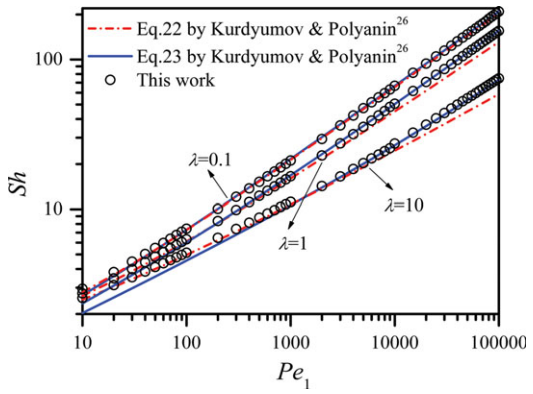

Figure 9. Variation of *Sh* with Pe_1 for mass transfer from a liquid drop in a uniaxial extensional flow.

[Color figure can be viewed in the online issue, which is available at wileyonlinelibrary.com.]

$$\overline{C}_{\mathrm{d}} = \frac{\int_0^1 \int_0^\pi C_2 r^2 \sin\theta dr d\theta}{\int_0^1 \int_0^\pi r^2 \sin\theta dr d\theta} = \frac{3}{2}\int_0^1 \int_0^\pi C_2 r^2 \sin\theta dr d\theta \qquad (31)$$

Equation 5 reveals that the internal velocity is proportional to $1/(\lambda + 1)$, so it is convenient to use a modified Peclet number, $Pe' = Pe_2/(\lambda + 1)$, to describe the relative strength of the convection to the diffusion inside the drop.[12,22] The variation of *Sh* with time is shown in Figure 11a, in which the Fourier number, $Fo = \tau Pe_2^{-1} = D_2 t/a^2$, is taken as the abscissa because it is proportional to the actual transport time for the same D_2. As expected in this figure, *Sh* increases with the increase of Pe' due to the enhancement of convective transport. Considering the mass transfer at given Pe', the variation of *Sh* with time can be approximately divided into three stages.[29] The first stage describes the initial process, where the molecular diffusion is dominant and *Sh* reduces rapidly at the same rate at different Pe'. The second stage is a transition period, in which the convective effect manifests itself gradually, and hence, *Sh* varies in a smoother manner at low Pe' but oscillates at high Pe'. The last stage indicates a quasi-steady process that *Sh* reaches an asymptotic value after a time long enough due to both the concentration gradient on the drop surface and the driving force decreasing in proportion. Figure 11b depicts the corresponding variation of $\overline{C}_{\mathrm{d}}$ with *Fo*. As one expects, the larger is Pe', the faster

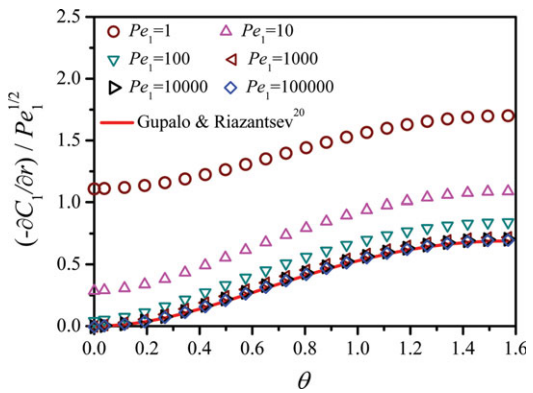

Figure 10. Local concentration gradient $(-\partial C_1/\partial r)/Pe_1^{1/2}$ on sphere surface as a function of θ at different Pe_1 for $\lambda = 1$ in a uniaxial extensional flow.

[Color figure can be viewed in the online issue, which is available at wileyonlinelibrary.com.]

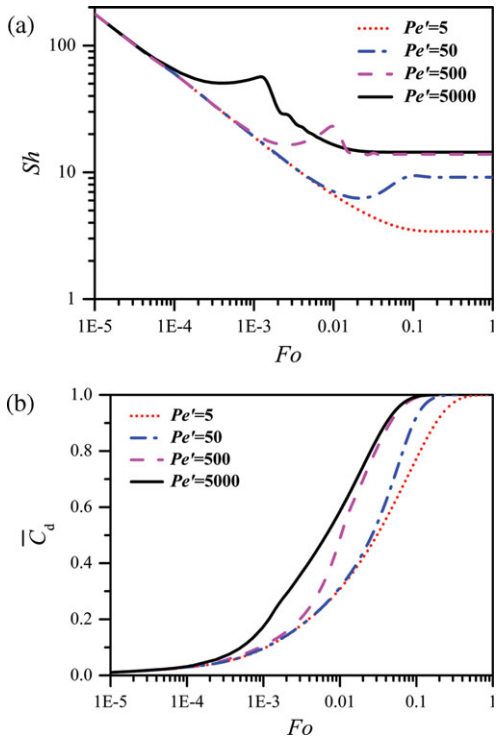

Figure 11. Transient transport behavior inside a drop for $\lambda = 1$ in a uniaxial extensional flow.

(a) Variation of *Sh* vs. *Fo* and (b) variation of $\overline{C}_{\mathrm{d}}$ vs. *Fo*. [Color figure can be viewed in the online issue, which is available at wileyonlinelibrary.com.]

increases $\overline{C}_{\mathrm{d}}$. In accordance with the behavior of *Sh* revealed in Figure 11a, $\overline{C}_{\mathrm{d}}$ increases rapidly at the same rate at different Pe' in the initial period, but after that the increase of $\overline{C}_{\mathrm{d}}$ becomes slower and eventually approaches unity.

Figure 12 depicts the concentration evolution inside a drop at different Pe'. As shown in Figure 12a, a thin diffusive boundary layer is formed near the drop surface at small *Fo* no matter Pe' is small or large because the diffusion is the dominant mechanism in the initial transport process. Thereafter, the convection resulted from the internal circulation begins to show its effect, so the concentration distribution is dissimilar at different Pe'. At small Pe', such as $Pe' = 1$ shown in Figure 12b, the diffusive transport perpendicular to the drop surface is predominant all the time, so the concentration contours are always roughly parallel to the surface though the concentration inside the drop keeps increasing with time. At large Pe', on the contrary, the solute passing through the initial diffusive boundary layer mainly moves along the internal streamlines due to the intensive convection. Thus, just as shown in Figure 12d at $Pe' = 5000$, the concentration contours become analogous to the flow structures eventually (see Figure 1b). Then, if we consider the transport process at some intermediate Peclet numbers, such as $Pe' = 50$ shown in Figure 12c, the diffusion and the convection compete with each other, and hence, the concentration contours are somehow a compromise between that for the diffusion-dominated case and that for the convection-dominated case.

As stated above that the transport process reaches a quasi-steady state and *Sh* approaches an asymptotic value Sh_∞ at last. Figure 13 depicts the variation of Sh_∞ with Pe', which reveals that Sh_∞ increases rapidly at some intermediate Pe' but then becomes weakly dependent on Pe' with further

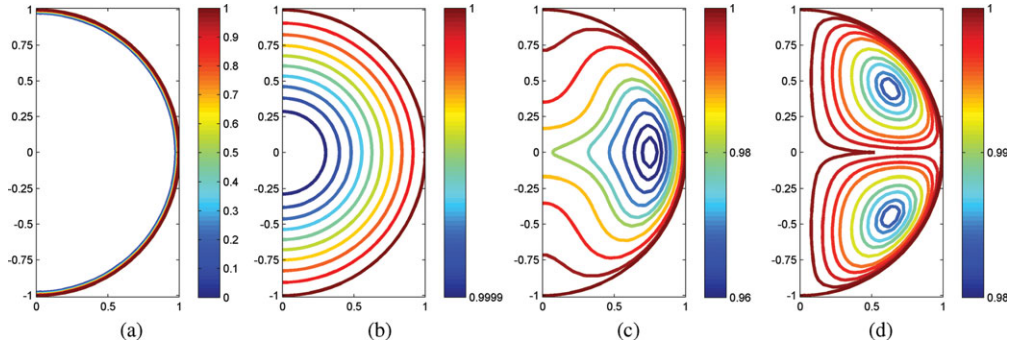

Figure 12. Concentration contours inside a drop in a uniaxial extensional flow.

(a) $Fo = 0.0001$ at various, Pe', (b) $Fo = 1$, $Pe' = 1$, (c) $Fo = 0.15$, $Pe' = 50$, and (d) $Fo = 0.1$, $Pe' = 5000$. [Color figure can be viewed in the online issue, which is available at wileyonlinelibrary.com.]

increasing Pe'. Sh_∞ reaches 14.6 when Pe' increases up to 100,000, which is already close to the limiting maximum value of 15 observed by Oliver et al.[30] for the heat transfer inside a drop suspended in an electric field because the internal circulation driven by a simple extensional field is similar to that driven by an electric field. On the other hand, Sh_∞ converges to the value of 3.29 as $Pe' \to 0$, which describes the pure diffusion case.[12] According to present simulations, one correlation applicable for predicting Sh_∞ in the range of $1 \le Pe' \le 100{,}000$ with a maximum error of 3% is derived as

$$Sh_\infty = 14.09 - \frac{10.87}{1+\left(\frac{Pe'}{45.81}\right)^{1.830}} \tag{32}$$

Sh_∞ denotes approximately the lower limit of mass-transfer rate in a given operating condition, so Eq. 32 can be used to evaluate a whole transport process roughly.

Another parameter that can be used to characterize a transient transport process is the time required for accomplishing some fraction of the total mass transfer. The time required for $\overline{C}_d$ increasing from the initial zero to 0.8 (80% of the total mass transfer), $Fo_{0.8}$, is given in Figure 14. It shows that $Fo_{0.8}$ decreases generally with increasing Pe', but the dependence of $Fo_{0.8}$ on Pe' is weak at small and high Pe'. In terms of present simulations, one correlation applicable for predicting $Fo_{0.8}$ in the range of $1 \le Fo_{0.8} \le 10{,}000$ with small relative deviations (<5%) is derived as

$$Fo_{0.8} = 0.026 + \frac{0.089}{1+\left(\frac{Pe'}{45.23}\right)^{1.521}} \tag{33}$$

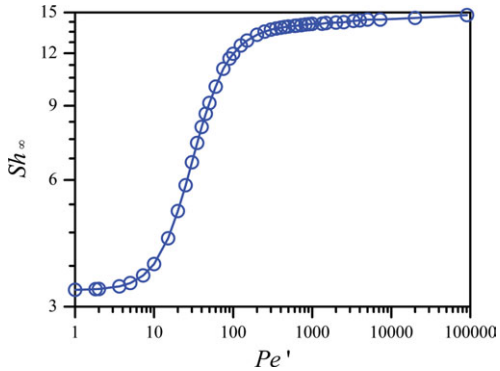

Figure 13. Variation of Sh_∞ with Pe' for a drop in a uniaxial extensional flow.

[Color figure can be viewed in the online issue, which is available at wileyonlinelibrary.com.]

It should be noted that all the above results for the internal mass transfer are just for the case of a spherical liquid drop immersed in the uniaxial extensional flow. With regard to the biaxial extension case, it is similar to the external transport process that Sh is equal to that in the uniaxial extension case. In comparison with Figure 12b, the concentration distribution for the biaxial extension case is shown in Figure 15 for a certain instant, which confirms the fact again that the flow direction has significant effect on the concentration distribution though it does not affect Sh.

Conclusions

The mass-transfer process both outside and inside a sphere immersed in a simple extensional flow is numerically investigated by making use of the known Stokes velocity field at small Reynolds numbers. A finite difference method with the control volume formulation is adopted to solve the advection-diffusion transport equation, in which a fifth-order WENO scheme is applied in spatial discretization and a third-order TVD Runge–Kutta scheme is applied in time.

For the mass transfer outside a sphere, our simulations show that the transport rate depends strongly on the Peclet number. Sh increases with the increase of Pe, but its dependency on Pe is associated with the physical property of the sphere. At high Pe, Sh is proportional to $Pe^{1/3}$ for a solid sphere, whereas it turns to be proportional to $Pe^{1/2}$ for a liquid drop. The value of viscosity ratio also affects the mass-transfer rate, and Sh decreases with the increase of λ because flow velocities are small at high λ.

For the transient mass transfer inside a drop, our simulations show the transport process can be divided into three stages:

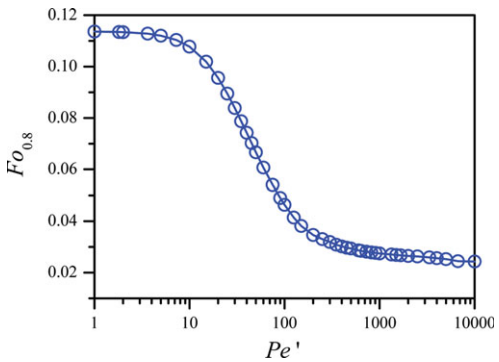

Figure 14. Variation of $Fo_{0.8}$ with Pe' for a drop in a uniaxial extensional flow.

[Color figure can be viewed in the online issue, which is available at wileyonlinelibrary.com.]

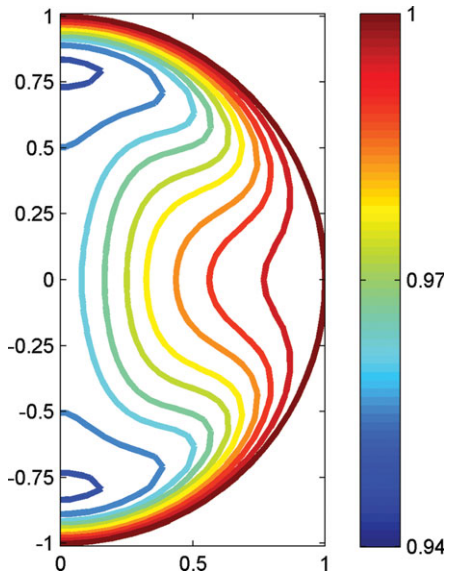

Figure 15. Concentration contours inside a drop at $Fo = 0.15$ and $Pe' = 50$ in a biaxial extensional flow.

[Color figure can be viewed in the online issue, which is available at wileyonlinelibrary.com.]

the diffusion-dominated, transitional, and quasi-steady transport stages. Sh also increases with increasing the modified Peclet number Pe'. With regard to the asymptotic Sh, it increases fast with Pe' at some intermediate ranges of Pe', whereas approaches the value of 3.29 for the pure diffusion as $Pe' \to 0$ and an approximate value of 15 as $Pe' \to \infty$. Correspondingly, the concentration inside the drop increases fast at high Pe' and the time required for accomplishing 80% of the total mass transfer decreases generally with increasing Pe'.

The simulation results in this work also confirm that the flow direction, no matter a uniaxial extensional flow or a biaxial one, has no effect on the total transfer rate but affects the concentration distribution significantly. The concentration distribution in a biaxial extension evolves in a contrary manner compared with that in a uniaxial extension due to the fluid flowing in the opposite directions.

Finally, as the equations and boundary conditions governing mass transfer are identical to those for heat transfer, the results in the former parts are also applicable to the relevant heat transfer problems. At any point, the corresponding correlations for heat transfer can be obtained by replacing solute concentration with temperature and molecular diffusivity with thermal diffusivity in those for mass transfer.

Acknowledgments

This work was supported by the National Basic Research Program of China (2009CB623406), the National Science Fund for Distinguished Young Scholars (21025627), the National Natural Science Foundation of China (20990224, 20676134), 863 Project (2011AA060704), Beijing Natural Science Foundation (5102030), and the Jiangsu Province Projects (BY2009133). The authors thank Professor Donald L. Koch at Cornell University a lot for his kind help and useful discussions on this work.

Literature Cited

1. Ward DM, Trass O, Johnson AI. Mass transfer from fluid and solid spheres at low Reynolds numbers. *Can J Chem Eng*. 1962;40:164–168.
2. Calderbank PH, Johnson DS, Loudon J. Velocity fields around spheres and bubbles investigated by laser-doppler anemometry. *Chem Eng Sci*. 1970;25:235–256.
3. Rowe PN, Claxton KT, Lewis JB. Heat and mass transfer from a single sphere in an extensive flowing fluid. *Trans Inst Chem Eng*. 1965;43:T14–T31.
4. Acrivos A, Taylor TD. Heat and mass transfer from single spheres in Stokes flow. *Phys Fluids*. 1962;5:387–394.
5. Levich VG, Krylov VS, Vorotilin VP. On the theory of unsteady diffusion from moving drops. *Trans Doklady Akademii Nauk SSSR*. 1965;161:648–651.
6. Ruckenstein E. Mass transfer between a single drop and a continuous phase. *Int J Heat Mass Transfer*. 1967;10:1785–1792.
7. Frankel NA, Acrivos A. Heat and mass transfer for small spheres and cylinders freely suspended in shear flow. *Phys Fluids*. 1968;11:1913–1918.
8. Chao BT. Transient heat and mass transfer to a translating droplet. *J Heat Transfer*. 1969;91:273–281.
9. Acrivos A. Heat transfer at high Peclet number from a small sphere freely rotating in a simple shear field. *J Fluid Mech*. 1971;46:233–240.
10. Poe GG, Acrivos A. Closed streamline flows past small rotating particles: heat transfer at high Peclet numbers. *Int J Multiphase Flow*. 1976;2:365–377.
11. Cooper F. Heat transfer from a sphere to an infinite medium. *Int J Heat Mass Transfer*. 1977;26:991–993.
12. Clift R, Grace JR, Weber ME. *Bubbles, Drops and Particles*. New York: Academic Press, 1978.
13. Subramanian G, Koch DL. Inertial effects on the transfer of heat or mass from neutrally buoyant spheres in a steady linear velocity field. *Phys Fluids*. 2006;18:073302.
14. Subramanian G, Koch DL. Centrifugal forces alter streamline topology and greatly enhance the rate of heat and mass transfer from neutrally buoyant particles to a shear flow. *Phys Rev Lett*. 2006;96:134503.
15. Feng ZG, Michaelides EE. A numerical study on the transient heat transfer from a sphere at high Reynolds and Peclet numbers. *Int J Heat Mass Transfer*. 2000;43:219–229.
16. Mao ZS, Li T, Chen J. Numerical simulation of steady and transient mass transfer to a single drop dominated by external resistance. *Int J Heat Mass Transfer*. 2001;44:1235–1247.
17. Waheed A, Henschke M, Pfennig A. Mass transfer by free and forced convection from single spherical liquid drops. *Int J Heat Mass Transfer*. 2002;45:4507–4514.
18. Li WZ, Yan YY, Smith JM. A numerical study of the interfacial transport characteristics outside spheroidal bubbles and solids. *Int J Multiphase Flow*. 2003;29:435–460.
19. Yang C, Zhang JS, Koch DL, Yin XL. Mass/heat transfer from a neutrally buoyant sphere in simple shear flow at finite Reynolds and Peclet numbers. *AIChE J*. 2011;57:1419–1433.
20. Gupalo YP, Riazantsev YS. Diffusion on a particle in the shear flow of a viscous fluid. Approximation of the diffusion boundary layer. *Appl Math Mech*. 1972;36:447–451.
21. Bachelor GK. Mass transfer from a particle suspended in fluid with a steady linear ambient velocity distribution. *J Fluid Mech*. 1979;95:369–400.
22. Morrison FA. Unsteady transport from a drop in axisymmetric straining flow. *Chem Eng Commun*. 1981;8:263–268.
23. Favelukis M, Semiat R. Mass transfer between a slender bubble and a viscous liquid in axisymmetric extensional flow. *Chem Eng Sci*. 1996;51:1169–1172.
24. Favelukis M. Unsteady mass transfer between a slender bubble and a viscous liquid in a simple extensional flow. *Can J Chem Eng*. 1998;76:959–963.
25. Favelukis M, Chiam SA. On the diffusion from a slender bubble in an extensional flow. *Chem Eng Commun*. 2003;190:475–488.
26. Kurdyumov VN, Polyanin AD. Mass transfer problem for particles, drops and bubbles in a shear flow. *Fluid Dyn*. 1990;25:611–615.
27. Leal LG.*Laminar Flow and Convective Transport Processes*. London: Butterworth-Heinemann, 1992.
28. Yang C, Mao ZS. Numerical simulation of interphase mass transfer with the level set approach. *Chem Eng Sci*. 2005;60:2643–2660.
29. Chung JN, Oliver DLR. Transient heat transfer in a fluid sphere translating in an electric field. *J Heat Transfer*. 1990;112:84–91.
30. Oliver DLR, Carleson TE, Chung JN. Transient heat transfer to a fluid sphere suspended in an electric field. *Int J Heat Mass Transfer*. 1985;28:1005–1009.

Manuscript received Apr. 10, 2011, revision received July 31, 2011, and final revision received Nov. 1, 2011.